Combustion and Flame 265 (2024) 113479

Contents lists available at ScienceDirect

Combustion and Flame

journal homepage: www.sciencedirect.com/journal/combustion-and-flame

Premixed flames in narrow heated channels of circular cross-section: Steady-state solutions, their linear stability analysis and the multiplicity of stable dynamic modes

Vadim N. Kurdyumov *, Daniel Fernández-Galisteo, Carmen Jiménez

Department of Energy, CIEMAT, Avda. Complutense 22, 28040 Madrid, Spain

ARTICLE INFO

Keywords:
Flame instabilities
Multiplicity of solutions
Micro combustion
Narrow-channel approximation

ABSTRACT

Premixed flames in narrow heated circular channels subjected to a Poiseuille flow are investigated within the constant density model for various Lewis numbers using irreversible one-step Arrhenius kinetics. A global stability analysis of steady-state axisymmetric solutions is carried out, together with time-dependent direct numerical simulations. The analysis reveals the criteria for the appearance of oscillatory and three-dimensional cellular flame structures. The problem is also studied separately within the framework of the narrow-channel approximation.

Among the results obtained, the following can be singled out as the main ones. First, the multiplicity of stable dynamic modes, oscillatory and steady-state, taking place for the same set of parameters for flames with $Le < 1$ is demonstrated. The actual occurrence of one mode or another depends on the initial conditions. Second, the appearance of chaotic regimes is shown for flames with $Le > 1$. The chaotic dynamics occurs in a narrow range of values of the flow rate, with Feigenbaum period-doubling cascades taking place both before and after this interval. The results of this study could be useful in the development and use of small-scale combustion devices.

Novelty and significance statement: A systematic study of premixed flames in narrow heated circular channels in the presence of Poiseuille flow is carried out for various Lewis numbers using irreversible one-step Arrhenius kinetics. One of the novelties presented in the paper is the linear global stability analysis of steady state axisymmetric solutions of this problem, which has not been reported before. Also, for the first time, the existence of multiple stable dynamic modes, oscillatory and time-independent, which occurs at the same parameter values, is demonstrated for flames with Lewis number smaller than one. For flames with a Lewis number greater than one, cases with chaotic dynamics are found that manifest themselves in a narrow range of the flow rate. Finally, it is demonstrated that the Feigenbaum cycle-doubling cascade can appear before and after this interval of chaotic dynamics. Such analysis has not been reported before for this problem of flames in partially heated channels.

1. Introduction

Understanding the structure and dynamics of flames in narrow channels is a necessary requisite when designing small-scale combustion devices, see general reviews [1–4]. This is the case, for example, of small scale superadiabatic burners, which present the particularity of reaching a temperature above the adiabatic temperature for a given mixture [5–9]. Superadiabatic burners, due to the effect of heat recirculation, are characterized by the possibility of allowing the burning of ultra-lean mixtures, that is, mixtures below the standard flammability limit [10–12]. This allows self-sustained combustion to occur for mixtures with low energy content. Reforming processes (for example, for the production of hydrogen), when the oxidant is in a very scarce amount, have a similar nature [13]. Another characteristic of these systems is that they are prone to developing instabilities of various types, which can lead to undesirable consequences, such as uncontrolled flame behavior or even flame extinction.

One canonical configuration for studying flame dynamics in narrow channels experimentally is an externally heated channel where only a part of the wall is heated. This turns out to be convenient for several reasons. One of the most important is that the flame location is confined to a region of the channel, preventing flame propagating upstream or downstream along the channel. Another advantage of this configuration

* Corresponding author.
E-mail address: vadim.k@ciemat.es (V.N. Kurdyumov).

https://doi.org/10.1016/j.combustflame.2024.113479
Received 29 November 2023; Received in revised form 20 April 2024; Accepted 22 April 2024
Available online 2 May 2024

is its capability to facilitate the study of the effect of heating on the complex chemical kinetics of the combustion process. Premixed flames in heated channel configurations have been investigated experimentally in [14–21]. In these studies, the emphasis was on studying the time-dependent flame dynamics [14,21] (in particular, FREI oscillations), the flame structures [16,19] and complex kinetics of chemical processes in flames [15,17]. The use of a micro-flow reactor with a controlled temperature profile is a convenient experimental tool. However, this system requires more detailed theoretical research.

Perhaps the main difficulty encountered in understanding the dynamics of combustion in channels lies in the simultaneous presence of various effects. Among them one can list the thermal interaction of the flame with the channel walls, the heat conduction inside the walls, the thermal expansion of the gas, or the differential diffusion effect. Although it is difficult to separate these effects experimentally, the numerical modeling analysis is able to separate them effectively, pointing the way for future experimental studies. An important obstacle is also the presence of a large number of parameters in the problem, which makes an exhaustive experimental study difficult. The development of simplified models permits to do parametric investigations in an effective way.

Heated channels have received some attention through numerical analysis [22–25]. In most of these studies, a fixed wall temperature distribution was assigned and an unexpectedly rich set of possible flame behaviors was demonstrated. In [22,23] the results of numerical simulations for hydrogen–air mixtures in narrow channels with a fixed temperature profile were reported. The influence of the Lewis number on the flame dynamics was studied on the basis of the one-step Arrhenius model in [24,25].

From the experimental point of view, imposing a given temperature to the wall is probably not very realistic: as the flame approaches the channel wall, the wall surface temperature can hardly be constant. Perhaps an exception would be the case of a channel wall made of a highly conductive material, which results in a temperature homogenization of the wall surface [26]. There are also obvious objective difficulties in measuring the temperature on the inner surface of the wall. For this reason, the possibility of doing numerical simulations is decisive in this kind of investigations.

According to the knowledge of the authors, the systematic study of flame dynamics in heated channels of circular cross section has not received due attention so far. In the present work, we assume that the temperature profile on the outer surface of the channel wall is controlled. Although this assumption may also raise doubts, it is probably much more realizable and experimentally verifiable than fixing the inner wall temperature, as was done in some studies [22–25]. A detailed study of heat transfer between the outer wall of the channel and the environment would certainly be an interesting topic, but consideration of this is beyond the scope of this work.

The article is structured as follows. The next section gives a mathematical formulation of the problem. The third section offers a brief description of the methods used in calculations. The fourth section is devoted to the description of steady-state axisymmetric solutions. In the fifth section, the results related to stability of axisymmetric solutions are given compared with time-dependent numerical simulations. The sixth section considers the limiting case of narrow channels. Finally, the last section presents a discussion of our results.

2. Mathematical formulation

The sketch of the problem under study is given in Fig. 1. Let us consider a combustible mixture at initial temperature T_0 and fuel mass fraction Y_{F0} flowing in a circular channel of radius R. The total mass flow rate through the channel, $\dot{M}$, is fixed. In what follows we use the standard cylindrical coordinates with z', r' and φ for the longitudinal, radial and angular coordinates, respectively, with t' denoting the time. Primes here and hereafter indicate dimensional quantities if the same notation is used for dimensional and non-dimensional variables.

Let the channel wall thickness be h_W. We assume that the temperature profile at the outer channel surface is a given function of z', namely $T|_{r'=R+h_W} = T_W(z')$. This assumption appears to be more realistic than setting the wall temperature as a whole, as has been done in some studies. Here, narrow channels with radius of the order of the thermal flame thickness are considered. If the wall thickness is small compared to the channel radius, $h_W/R \ll 1$, the temperature across the wall can be approximated by a linear with r' profile. Thus, the radial heat flux through the wall is determined by the temperature difference between the interior and the exterior surfaces of the wall.

This study deals with a diffusive-thermal or "constant-density" model, according to which the density of the mixture ρ, the heat capacity c_p, the thermal diffusivity D_T, and the molecular diffusivity D are all assumed constant. Consequently, the flow field, unaffected by the combustion process, is given by the Poiseuille flow: $u_z = 2\,U_0[1 - (r'/R)^2]$ and $u_r = u_\varphi = 0$, where $U_0 = \dot{M}/\pi\rho R^2$ is the mean flow velocity value.

In the following, we use a simplified kinetics where the combustible mixture undergoes a chemical reaction modeled by a global irreversible step $F + O \to P + Q$. Here F, O and P denote the fuel, the oxidizer and the products, respectively, and Q is the heat released per unit mass of fuel. Assuming that the mixture is lean in fuel, the oxidizer mass fraction remains nearly constant and the reaction rate is modeled by an Arrhenius law $\Omega = \mathcal{B}\rho^2 Y_F \exp(-\mathcal{E}/\mathcal{R}T)$, where $\mathcal{B}$ is a pre-exponential factor containing Y_O and the molecular weights. Of course, one can consider an equivalent situation where the oxidizer represents a deficient component, as happens when rich mixtures are burned.

The burning speed evaluated at $T = T_0$ of the corresponding planar deflagration wave, S_L, and the thermal flame thickness defined as $\delta_T = D_T/S_L$ are used below to specify the non-dimensional parameters. The non-dimensional temperature is defined as $\theta = (T - T_0)/(T_e - T_0)$, where $T_e = T_0 + QY_{F0}/c_p$ is the adiabatic temperature of the planar flame based on the unburned gas temperature T_0 and the upstream fuel mass fraction Y_{F0}. Choosing δ_T and R as the reference length scales for the z and r directions, respectively, δ_T^2/D_T as the time scale, $(z, r) = (z'/\delta_T, r'/R)$, $t = t'D_T/\delta_T^2$, and Y_{F0} to normalize the fuel mass fraction, $Y = Y_F/Y_{F0}$, the dimensionless equations written in the moving reference frame become

$$\frac{\partial\theta}{\partial t} + 2\,m(1-r^2)\frac{\partial\theta}{\partial z} = \frac{\partial^2\theta}{\partial z^2} + \frac{1}{a^2}\Delta_{r\varphi}\theta + \omega\,, \tag{1}$$

$$\frac{\partial Y}{\partial t} + 2\,m(1-r^2)\frac{\partial Y}{\partial z} = \frac{1}{Le}\left(\frac{\partial^2 Y}{\partial z^2} + \frac{1}{a^2}\Delta_{r\varphi}Y\right) - \omega\,, \tag{2}$$

where $\Delta_{r\varphi} = \partial^2/\partial r^2 + r^{-1}\partial/\partial r + r^{-2}\partial^2/\partial\varphi^2$ and

$$\omega = \frac{\beta^2}{2Le\,u_p^2} Y \exp\left\{\frac{\beta(\theta-1)}{1+\gamma(\theta-1)}\right\}. \tag{3}$$

Eqs. (1) and (2) are to be solved subject to the following boundary conditions. The functions θ and Y are 2π-periodic functions of φ. Using the linearity of the radial temperature distribution inside the wall, the dimensionless temperature and no-flux mass fraction conditions at the wall lead to

$$r = 1: \quad \partial\theta/\partial r = -\frac{1}{2}\,a^2\,b\cdot[\theta - \theta_W(z)]\,, \quad \partial Y/\partial r = 0, \tag{4}$$

where $\theta_W(z) = (T_W(z) - T_0)/(T_e - T_0)$ is the dimensionless temperature profile fixed on the outer surface of the channel wall. Here

$$b = 2\frac{\lambda_W}{\lambda}\cdot\frac{\delta_T^2}{R\,h_W} \tag{5}$$

is the heat transfer parameter, where λ_W is the wall thermal conductivity coefficient. It can be seen that as $b \to \infty$, the temperature boundary condition (4) transforms into a condition with a fixed temperature profile at the inner wall surface.

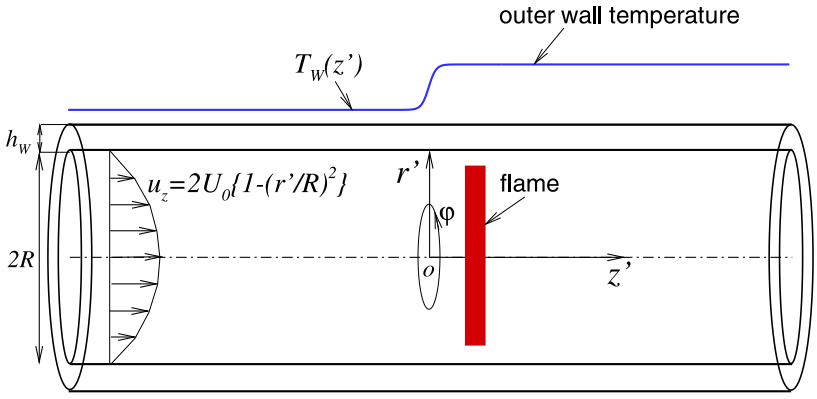

Fig. 1. Sketch of the problem under study, coordinate system, the outer wall temperature and flow velocity profiles.

The parameter $a = R/\delta_T$ appearing in Eqs. (1)–(2) and (4) represents the dimensionless channel radius measured with the thermal width of the planar flame. The purpose of writing these equations in this form is related with the limiting case of very narrow channels, in order to compare the results for $a = O(1)$ and $a \to 0$. It should be noted, however, that the representation of the boundary conditions in the form of Eq. (4) is useful only for $a \lesssim 1$. For cases $a \gg 1$, it is better to use the standard form $\tilde{b} = b \cdot a = 2(\lambda_w/\lambda)(\delta_T/h_W)$ for the dimensionless heat transfer parameter.

For axisymmetric calculations, namely when $\partial/\partial\varphi \equiv 0$ is imposed, the standard symmetry conditions are used at the axis

$$r = 0: \quad \partial\theta/\partial r = \partial Y/\partial r = 0. \tag{6}$$

In cases of three-dimensional calculations, when the azimuthal coordinate φ is taken into account, a procedure implying the absence of any physical singularity at the axis is used for the temperature and mass fraction fields [27,28]. This procedure, which affects the numerical treatment of the Laplace operator appearing in Eqs. (1)–(2) near the axis, was described in the Appendix of [27].

The temperature and the fuel mass fraction take their prescribed upstream values

$$Y = 1, \quad \theta = 0 \quad \text{as} \quad z \to -\infty. \tag{7}$$

For outlet boundary condition we require

$$\partial^2\theta/\partial z^2 = \partial^2 Y/\partial z^2 = 0 \quad \text{as} \quad z \to +\infty. \tag{8}$$

These weak or mild outlet boundary conditions were used in [29] for cases with heat losses included, reducing in this way the computational domain. The numerical simulations reported below showed that the influence of the downstream boundary condition becomes negligible, as it should be, if the size of the computational domain is reasonably long downstream the flame.

In general, any temperature profile on the outer wall of the channel can be controlled under experimental conditions. For simplicity, in most cases, we defined the temperature profile on the outer wall using the Heaviside step function,

$$\theta_W(z) = \theta_w \cdot \mathrm{Hev}(z), \tag{9}$$

where $\mathrm{Hev}(z \le 0) = 0$, $\mathrm{Hev}(z > 0) = 1$ and θ_w is kept constant. However, for the purpose of showing that the results are robust with respect to the external temperature profile, a second profile

$$\theta_W(z) = \theta_w \cdot [1 + \tanh(z/\ell)]/2, \tag{10}$$

will also be applied in some cases. Here ℓ defines the dimensionless extent of the smoothing of a sharp step of the wall temperature measured in terms of δ_T.

Thus, the following non-dimensional parameters appear in the above equations: the dimensionless channel radius, $a = R/\delta_T$, the Zel'dovich number, $\beta = \mathcal{E}(T_a - T_0)/RT_a^2$, the Lewis number, $Le = \lambda/\rho c_p D$, the heat release parameter, $\gamma = (T_a - T_0)/T_a$, the nondimensional flow rate, $m = U_0/S_L$, normalized with the planar flame speed, S_L, and the heat transfer parameter b given by Eq. (5).

The factor $u_p = S_L/U_L$ appearing in Eq. (3) has been introduced to account for the difference between the asymptotic value of the laminar flame speed,

$$U_L = \sqrt{2\rho\mathcal{B}\mathcal{D}_T Le\beta^{-2}}\exp(-\mathcal{E}/2RT_e),$$

obtained for large activation energy ($\beta \gg 1$) and the numerical value S_L calculated for a finite β, see [30]. Clearly, the factor u_p tends to unity when $\beta \to \infty$. The numerical values of u_p were reported in [31] as a function of the Lewis number for $\beta = 10$ and $\gamma = 0.7$. These values are kept as representative values in the present study, unless otherwise stated.

2.1. Narrow-channel approximation

For completeness, the narrow channel approximation is given below. The equation determining the boundary condition at the inner channel surface is written in a form that allows to consider the limiting case $a \to 0$. To do this, all variables are expanded in power series of a^2, namely, in the form $f = f_0 + a^2 f_1 + \ldots$, where f stands for the temperature or the mass fraction. To leading order $\Delta_{r\varphi}\theta_0 = 0$, $\Delta_{r\varphi}Y_0 = 0$, which implies $\theta_0 = \theta_0(z)$, $Y_0 = Y_0(z)$.

It can be seen that substitution of the two-term expansions in a^2 into Eq. (4) gives

$$r = 1: \quad \partial\theta_1/\partial r = -\frac{1}{2}\, b \cdot [\theta_0 - \theta_W(z)], \quad \partial Y_1/\partial r = 0. \tag{11}$$

Substituting then the two-term expansions into Eqs. (1)–(2) and integrating over the channel cross-section, we obtain the limit equations for $a \ll 1$:

$$\frac{\partial\theta_0}{\partial t} + m\frac{\partial\theta_0}{\partial z} = \frac{\partial^2\theta_0}{\partial z^2} + \omega(\theta_0, Y_0) - b \cdot [\theta_0 - \theta_W(z)], \tag{12}$$

$$\frac{\partial Y_0}{\partial t} + m\frac{\partial Y_0}{\partial z} = \frac{1}{Le}\frac{\partial^2 Y_0}{\partial z^2} - \omega(\theta_0, Y_0), \tag{13}$$

where Eq. (11) was used. When further referring to the limit $a \to 0$, the index "0" will be omitted. It should be noted that the heat transfer coefficient b appearing in Eqs. (4) and (12) is the same effective coefficient that allows one to estimate the influence of the channel radius on the flame behavior. The boundary conditions for Eqs. (12)–(13) are given by Eqs. (7)–(8). Thus, it can be seen that the factor 2 was included in the definition of the dimensionless heat exchange coefficient b given by Eq. (5) so that in the limit $a \to 0$ the heat exchange term takes the form as shown in Eq. (12).

3. Numerical treatment

The numerical procedures used in the present study are similar to those applied in [28], where the combustion wave in a channel of circular cross section was considered. However, in the essence of the subject, the difference in the formulations is obvious. In [28], freely propagating flames in adiabatic channels were studied, while in the present work the flame is stabilized at some location due to the wall heating.

3.1. Steady-state and time-dependent solutions

Steady as well as time-dependent computations were carried out in a finite domain, $z_{min} < z < z_{max}$, with typical values $z_{min} = -50$ and $z_{max} = 50$. The size of the domain was significantly varied in order to check the independence of the results. In particular, there was a need to increase the upstream domain segment ($z_{min} < z < 0$) at low values of the flow rate m.

The spatial derivatives were discretized on a uniform grid using second-order, three-point central differences. The typical number of grid points was about 2001 for one-dimensional calculations, 1001×101 for two-dimensional calculations and $501 \times 51 \times 81$ for three-dimensional ones. The number of grid points was doubled in some cases without significant differences in results. Particular attention was paid to verify that the downstream boundary conditions given by Eq. (8) do not affect the resulting numerical solution, in particular the position of the flame.

In order to determine steady state (but not necessary stable) axisymmetric solutions, the steady counterparts ($\partial/\partial t = 0$) of Eqs. (1) and (2) were solved using a Gauss–Seidel method with over-relaxation. For unsteady calculations an explicit marching procedure was used with first order discretization in time. The typical time step was varied from $\tau = 10^{-4}$ to 10^{-5}. No significant differences were found in the results when τ was halved.

1D and 2D (axisymmetric) simulations were carried out as well. In the first case, the initial conditions were chosen in the form of distributions independent of the transverse coordinate,

$$t = 0: \quad \theta = [1 + \tanh(\xi)]/2, \quad Y = [1 - \tanh(\xi)]/2,$$

where $\xi = (z - c_1)/c_2$ with c_1 and c_2 of order unity. It should be noted that although the initial stage of the numerical dynamics resulted dependent on these values, after a transition time the flame dynamics became independent of these specific values.

A number of 3D numerical simulations was carried out. As initial conditions, the corresponding steady-state axisymmetric distribution was chosen for the mass fraction, but for the temperature field the initial distribution was perturbed for $t = 0$ as

$$\theta = \theta_0(r,z) + \sum_{k=1}^{K} A_k \exp\left\{ -\frac{\sqrt{(z-z_k)^2 + a^2(r\cos\varphi - x_k)^2 + a^2(r\sin\varphi - y_k)^2}}{d_k} \right\}. \quad (14)$$

Here $\theta_0(r,z)$ is the axisymmetric steady-state temperature distribution, A_k is the perturbation amplitude, (x_k, y_k, z_k) is the position of the kth center of a perturbation profile in the channel, and d_k is its characteristic width. The typical values of A_k and d_k were usually chosen of the order of 0.1 and 1, respectively, and K varied from 1 to 3. It should be noted that three-dimensional calculations resulted to be expensive from a numerical point of view due to the need to carry out them to large times in order to investigate the established flame dynamics.

Visual identifications of the 3D flame structure are difficult in some cases. In order to facilitate the structural analysis, the following tool was used. The temperature field was presented in terms of the Fourier series

$$\theta(z,r,\varphi,t) = \overline{\theta} + \sum_{n=1}^{\infty} (a_n \cos n\varphi + b_n \sin n\varphi), \quad (15)$$

where all a_n and b_n are functions of z, r and t. Upon this, the functions F_n were calculated as follows

$$F_n(z,t) = \int_0^1 r\sqrt{a_n^2 + b_n^2}\, dr, \quad n \geq 1. \quad (16)$$

Here $\overline{\theta} = (2\pi)^{-1} \int_0^{2\pi} \theta d\varphi$ is the φ-averaged temperature and $F_n(z,t)$ characterizes the weight of the non-axisymmetric mode n in the solution. Clearly, all F_n are zero (within numerical accuracy) for an axisymmetric solution, but assume appreciably nonzero values when the solution is non-axisymmetric. In addition to this, the resulting distributions of the F_n function make it possible to determine which modes are dominant from the point of view of axial symmetry.

In the present study, the flame position, z_f, is defined as a point along the axis, $r = 0$, at which the reaction rate ω reaches its maximum value. It is also useful to determine a surface $z = Z_f(r,\varphi,t)$ on which the reaction rate reaches its maximum value along a line parallel to the axis. Thus, $z_f = Z_f(r,\varphi,t)|_{r=0}$. In the case of axisymmetric solutions ($\partial/\partial\varphi \equiv 0$), we use also the point with the maximum reaction rate along the wall, $z_f^w = Z_f(r,t)|_{r=1}$.

3.2. Stability analysis method

The method applied for the stability analysis is similar to that used in [27–29,31]. For the sake of completeness, it is described briefly below. The axisymmetric solutions described in the previous section have been examined for linear stability. The distributions of the steady-state temperature and mass fraction, all now denoted by subindex "0", are perturbed as usual with small perturbations

$$\begin{aligned} \theta &= \theta_0(z,r) + \epsilon\Phi(z,r)\exp(\lambda t + i\, n\, \varphi), \\ Y &= Y_0(z,r) + \epsilon\Psi(z,r)\exp(\lambda t + i\, n\, \varphi), \end{aligned} \quad (17)$$

where λ is a complex number, the real part of which represents the growth rate, $n = 0, 1, 2, \ldots$ is the azimuthal wave number and ϵ is a small amplitude. The mode $n = 0$ represents axisymmetric perturbations.

The linearized eigenvalue problem obtained when substituting Eq. (17) into Eqs (1)–(2) reduces to finding non-trivial solutions of the two-dimensional system

$$\lambda\Phi = -2m(1-r^2)\frac{\partial\Phi}{\partial z} + \frac{\partial^2\Phi}{\partial z^2} + \mathcal{L}\Phi + (A\Phi + B\Psi), \quad (18)$$

$$\lambda\Psi = -2m(1-r^2)\frac{\partial\Psi}{\partial z} + Le^{-1}\frac{\partial^2\Psi}{\partial z^2} + Le^{-1}\mathcal{L}\Psi - (A\Phi + B\Psi), \quad (19)$$

where $\mathcal{L} = a^{-2}(\partial^2/\partial r^2 + r^{-1}\partial/\partial r - n^2 r^{-2})$ and

$$\begin{aligned} A &= \frac{\partial\omega(Y_0,\theta_0)}{\partial\theta_0} = \frac{\beta^3 Y_0}{2Le\, u_p^2[1+\gamma(\theta_0-1)]^2}\exp\left\{\frac{\beta(\theta_0-1)}{1+\gamma(\theta_0-1)}\right\}, \\ B &= \frac{\partial\omega(Y_0,\theta_0)}{\partial Y_0} = \frac{\beta^2}{2Le\, u_p^2}\exp\left\{\frac{\beta(\theta_0-1)}{1+\gamma(\theta_0-1)}\right\}. \end{aligned} \quad (20)$$

Note that A and B are both functions of z and r.

Eqs. (18)–(19) should be supplemented by the following boundary conditions. At the wall we require

$$r = 1: \quad \partial\Phi/\partial r = -\frac{1}{2}a^2 b\cdot\Phi, \quad \partial\Psi/\partial r = 0. \quad (21)$$

The following conditions should be imposed at the axis

$$r = 0: \quad \begin{aligned} \partial\Phi/\partial r = \partial\Psi/\partial r = 0, &\quad \text{for} \quad n = 0, \\ \Phi = \Psi = 0, &\quad \text{for} \quad n > 0. \end{aligned} \quad (22)$$

The difference in the boundary conditions on the channel axis for modes with $n = 0$ and $n > 0$ is obtained from inspecting the eigenfunction behavior at small r. Indeed, it can be shown that $\Psi \sim \Phi \sim r^n$ since the leading terms in Eqs. (18)–(19) are $\mathcal{L}\Phi = 0$ and $\mathcal{L}\Psi = 0$ at $r \to 0$.

Far upstream and downstream the boundary conditions are given by

$$z \to -\infty: \quad \Phi = \Psi = 0; \quad z \to +\infty: \quad \partial^2\Phi/\partial z^2 = \partial^2\Psi/\partial z^2 = 0. \quad (23)$$

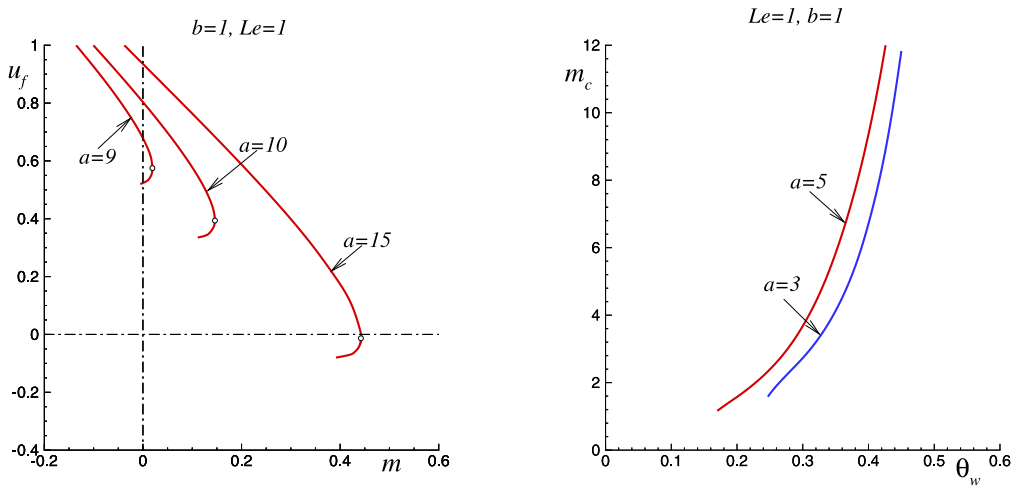

Fig. 2. Flame propagation in a channel with a uniform temperature of the outer wall, $\theta_W(z) = \theta_w$. Left plot: the dependence of axisymmetric flame speed in a channel with $\theta_w = 0$ on the flow rate, for $b = 1$, $Le = 1$ and various a. Propagation upstream ($u_f > 0$) is impossible to the right of the turning points (open circles). Right plot: the critical flow rate, m_c, plotted versus the outer wall temperature, θ_w, calculated for $a = 3$ and 5 with $Le = 1$ and $b = 1$. The flame is blown away downstream for $m > m_c$.

In the same manner reported in [28,31], the eigenvalue with a largest real part, or the main eigenvalue, was calculated. If the real part of this eigenvalue is positive, $\lambda_R = \Re(\lambda_1) > 0$, then the steady state is unstable, and conversely, if it is non-positive, $\lambda_R = \Re(\lambda_1) \le 0$, the steady state is linearly stable. The imaginary part of this eigenvalue, $\lambda_I = \Im(\lambda_1)$, represents the frequency of oscillations. It is important to underline that obtaining the main eigenvalue of the problem completely answers the question of whether the corresponding steady-state solution is stable or not.

4. Steady-state axisymmetric flames

4.1. Blow-off and flash-back conditions

Before describing the steady-state results, the following details should be noted. Although the temperature of the outer wall surface is kept hot and constant for $z > 0$, there is a critical value of the flow rate above which the flame will be blown off downstream. This value depends on the parameters of the problem, in particular on the channel radius, a, and the heat transfer coefficient, b. To find this critical value, it is necessary to consider the case of a freely propagating flame in a channel with a uniform temperature of the outer wall, namely, to set the wall boundary condition given by Eq. (4) using $\theta_W(z) = \theta_w$, where $\theta_w = const$, for $-\infty < z < \infty$. Writing down the governing equations in a moving frame of reference, $x \to x + u_f \cdot t$, and then considering $\partial/\partial t \equiv 0$, the value of u_f becomes an eigenvalue of the problem to be solved. The flashback point, or the value of the flow rate $m = m_c$ at which the flame is motionless relative to the wall, $u_f = 0$, determines this critical value. Apparently, this problem was not considered when setting the temperature profile on the outer surface of the channel by means of Eq. (11). Nevertheless, the present study does not aim at a detailed study of this item. For adiabatic conditions on the inner channel surface, (imposing $b = 0$ in Eq. (4)) this problem was considered, for example, in [28]. Here we confine ourselves only to the case with $Le = 1$. Let us only note, however, that the blow-off condition essentially depends on the Lewis number and that non-axisymmetric flames with faster propagation speeds can appear for $Le < 1$, e.g. [28,31,32].

Fig. 2 (right) illustrates the values of m_c plotted versus θ_w calculated with $a = 3$ and $a = 5$ for $Le = 1$ and $b = 1$. It can be seen that m_c increases rapidly with increasing values of θ_w. In the present study, θ_w is varied from 0.4 to 0.6 and the considered values of m (about $0 < m < 3$) are appreciably lower than the critical values corresponding to $\theta_w = 0.4$ ($m > 6$).

The external wall surface temperature is also maintained constant (cold) for $z < 0$. Theoretically, the flame can move upstream (leftward) if the flow rate is smaller than a certain value. Fig. 2 (left) shows the axisymmetric combustion front speed calculated for $b = 1$ and $Le = 1$ plotted as a function of the flow rate. All curves have a typical C-shape in which the lower branch of solutions is unstable and the upper branch is stable. The turning points are marked with open circles. The upstream flame propagation corresponds to $u_f > 0$. There are no solutions corresponding to the flame freely propagating upstream to the right of the turning point. Thus, for $\theta_w = 0$, the critical radius value (open circles) rapidly decreases. For $a \approx 8.8$, the turning point is located at $m \approx 0$ and upstream flame propagation with flow rate $m \ge 0$ becomes impossible at $a < 8.8$ (for $Le = 1$ and $b = 1$). In the present study, for all the considered cases, the radius is sufficiently small to avoid upstream flame propagation.

4.2. Steady-state results

Consider the steady-state axisymmetric solutions obtained imposing $\partial/\partial t = \partial/\partial\varphi = 0$ in Eqs. (1)–(2). Anticipating the results of the stability analysis, not all of these solutions are stable. However, knowledge of the steady-state solutions, even unstable ones, allows to better understand the influence of parameters on the flame structure and dynamics.

The changes in the flame structure with the Lewis number are illustrated in Fig. 3 for $m = 1$, $a = 5$, $b = 1$ and $\theta_w = 0.6$. The colored shadings show the temperature field while the isolines represent the reaction rate plotted for $\omega = 0.1$, 0.5, 1 and 2. It can be seen that for $Le < 1$ (upper plot) the peak of the reaction rate is located at a distance from the channel axis. Proximity to the wall leads to a decrease of the temperature in the reaction zone. As the Lewis number increases, the reaction rate peak moves toward the channel axis. Besides, at large Lewis numbers, the flame profile becomes almost planar near the axis, as the case with $Le = 4$ shows (lower plot).

Fig. 4 shows, as functions of the flow rate m, the flame position on the axis (left plot) and the maximum temperature reached in the domain (right plot), calculated for $a = 5$, $b = 1$, $\theta_w = 0.6$ and different Lewis numbers. It can be seen in the left figure that the curves z_f versus m are qualitatively similar despite the difference in the Lewis number.

This non-monotonic behavior of the steady-state flame position with a gradual increase of the flow rate is not a new effect. For example, a similar behavior was observed for flames stabilized near a porous-plug burner maintained at a constant temperature, see [33,34]. Intuitively, one would assume that as the flow rate increases, the steady-state flame

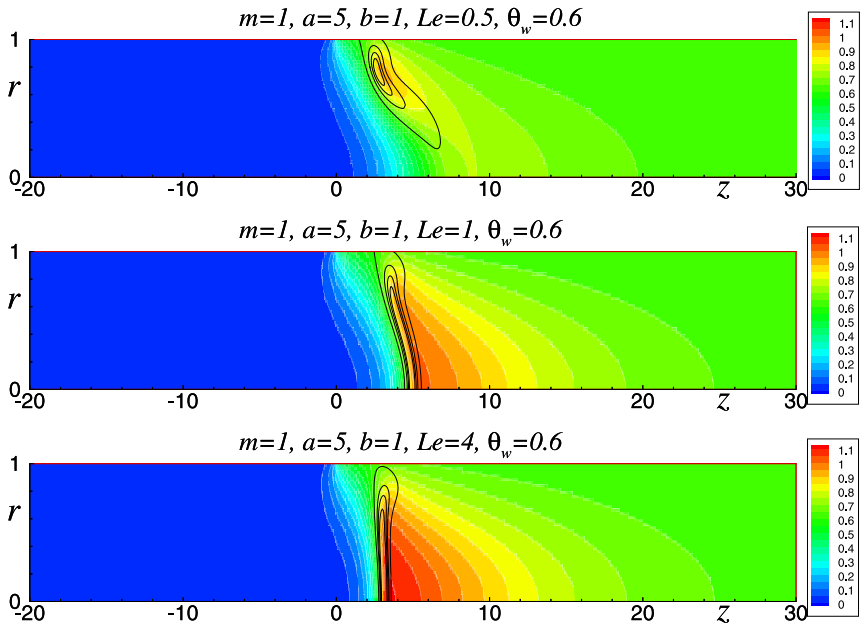

Fig. 3. Examples of temperature (color plot) and reaction rates (isolines) distributions calculated for $m = 1$, $a = 5$, $b = 1$ and various Lewis number; the isolines are shown for $\omega = 0.1$, 0.5, 1 and 2.

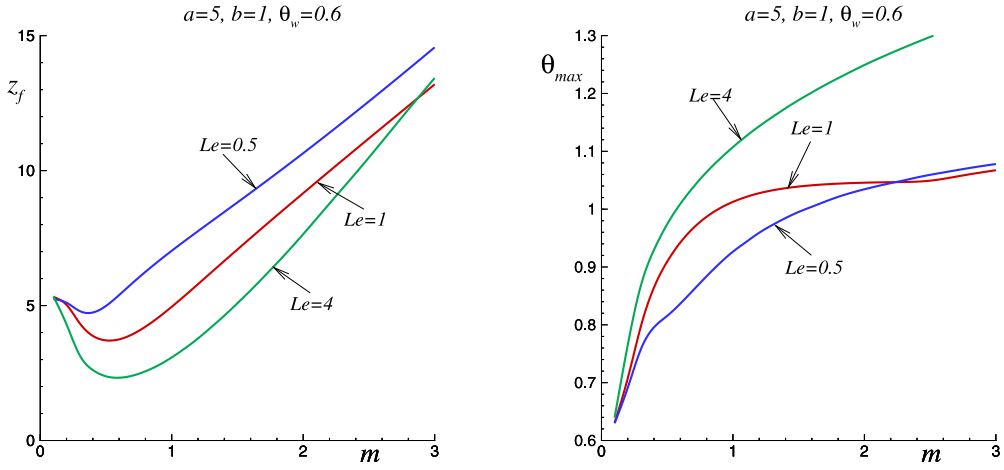

Fig. 4. The position of the flame on the channel axis (left plot) and the maximum temperature reached in the domain (right plot) as a function of the flow rate, for $a = 5$, $b = 1$, $\theta_w = 0.6$ and various Lewis numbers.

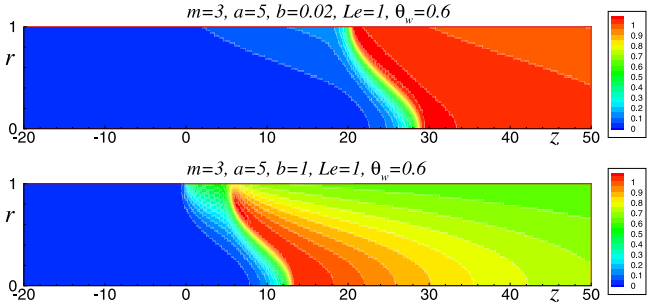

Fig. 5. Examples of temperature distributions for the cases $b = 0.02$ (upper plot) and $b = 1$ (lower plot), for $m = 3$, $a = 5$ and $Le = 1$.

position should move downstream monotonically due to the increasing convection effect. However, a low flow rate provides only a small amount of fuel delivering to the combustion zone. As a result, the flame is weak and it can only be located quite far downstream from the beginning of the heating zone due to heat losses. With an increase of m, an increase in the fuel supply produces stronger flames which can move upstream. However, with further increase in m, the flame again shifts downstream due to increased convective drift.

The flame structures calculated for $b = 0.02$ and $b = 1$ are illustrated in Fig. 5 for $m = 3$, $a = 5$ and $Le = 1$. The corresponding temperature

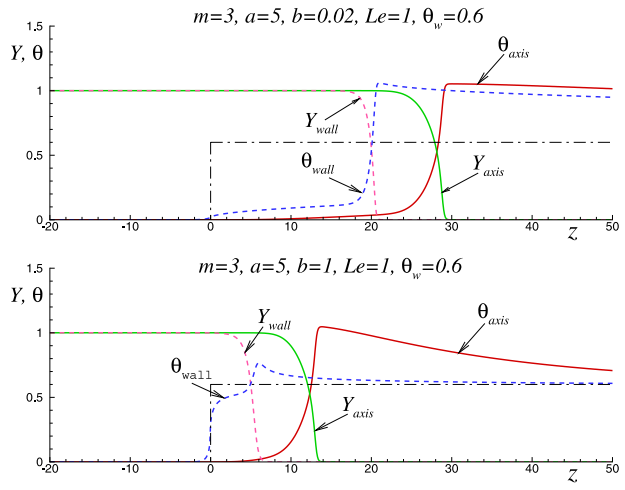

Fig. 6. Temperature and mass fraction distributions along the channel axis (solid lines) and along the wall (dashed lines) calculated for $b = 0.02$ and $b = 1$; the dash-dotted lines show the temperature on the outer side of the wall.

and mass fraction distributions along the channel axis (solid lines) and along the wall (dashed lines) are shown in Fig. 6. As expected, at low values of b, a longer distance is required to reach a temperature sufficient for mixture burning.

The influence of other parameters on the steady-state flame position was also investigated. Fig. 7 (left plot) presents z_f as a function of the flow rate m for different values of the coefficient b. All curves are plotted for $a = 5$, $\theta_w = 0.6$ and $Le = 1$. It can be seen that with a decrease in b, the minimum value of the flame position also decreases, approaching the beginning of the heating zone $z = 0$. The flame position z_f versus the flow rate m is drawn in Fig. 7 (right plot) for different values of θ_w, for $a = 5$, $Le = 1$ and $b = 0.02$. As expected, as the heating temperature decreases, the flame shifts downstream.

It should be noted that at low values of θ_w, in addition to the combustion mode characterized by a relatively narrow reaction zone of fuel consumption, there is another steady-state solution of Eqs. (1)–(2) characterized by a very slow chemical reaction. Strictly speaking, this mode cannot be classified as a combustion regime, although the reaction rate also reaches its maximum value along the channel axis. This branch is indicated with a dashed line in Fig. 8 for $\theta_w = 0.4$ where the standard combustion mode is also shown by a solid line. The temperature and mass fraction profiles along the axis corresponding to the open circles in Fig. 8 are drawn in Fig. 9. The upper plot illustrates the combustion regime corresponding to the circle on the solid curve in Fig. 8, the normal combustion mode, while the lower plot illustrates a low reaction rate mode corresponding to the circle on the dashed line. It is evident that a slow fuel conversion into products is presented for the latter case. It is interesting to note that for the combustion regime illustrated in the upper plot of Fig. 9, incomplete fuel consumption occurs due to the low temperature in the reaction region near the wall. Apparently, the regime with a slow chemical reaction at low heating temperatures can be classified as a cold flame. It is also obvious that this solution must strongly depend on the Zel'dovich number.

Quite often in studies of flame dynamics in channels, the narrow-channel approximation is used. As the dimensionless channel radius $a = R/\delta_T$ decreases, the solutions of Eqs. (1)–(2) become independent on r, approaching the limit case $a \to 0$ described by Eqs. (12)–(13). Fig. 10 shows with solid lines the dependence of the position of the flame on the channel axis, z_f, versus m for various decreasing values of a. The curves for z_f^w, the position of the flame near the channel wall, are drawn with a long-dashed line for $a = 3$, with a dashed line for $a = 2$ and with a dash-dotted line for $a = 1$. The open triangles in this figure show the flame position in the limiting case $a \to 0$ (for which $z_f = z_f^w$). This result demonstrates that for $a \lesssim 1$ the difference of the flame positions at the axis and at the wall becomes really small and the one-dimensional approximation given by Eqs. (12)–(13) describes the flame structure satisfactorily.

5. Stability analysis versus unsteady calculations

Although the steady-state axisymmetric flame structures described above appear to be qualitatively similar for different Lewis numbers as the flow rate changes, the stability properties turn out to be noticeably different. To facilitate understanding, it is worth starting the presentation with the case of Lewis number equal to unity when there is no differential diffusion effect.

5.1. Flames with $Le = 1$

As the dimensionless channel radius decreases, not only the steady-state solutions approach that of the $a \to 0$ limit based on Eqs. (12)–(13),

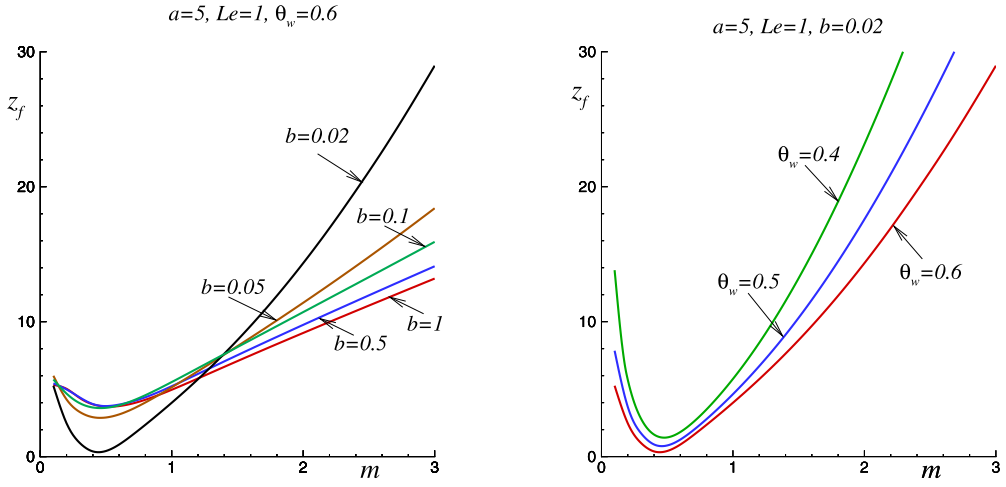

Fig. 7. Left plot: the flame position z_f as a function of the flow rate m for different values of b; all curves are plotted for $a = 5$, $\theta_w = 0.6$ and $Le = 1$. Right plot: the flame position as a function of m for various θ_w, plotted for $a = 5$, $b = 0.02$ and $Le = 1$.

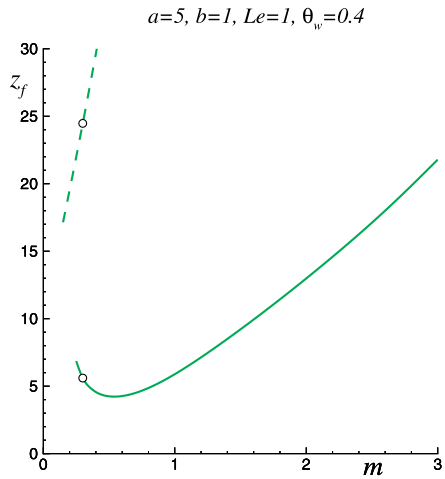

Fig. 8. Dependence of the position of the maximum reaction rate ω_{max} on the channel axis for the combustion mode (solid line) and the slow reaction mode (dashed line), for $a = 5$, $b = 1$, $Le = 1$ and $\theta_w = 0.4$.

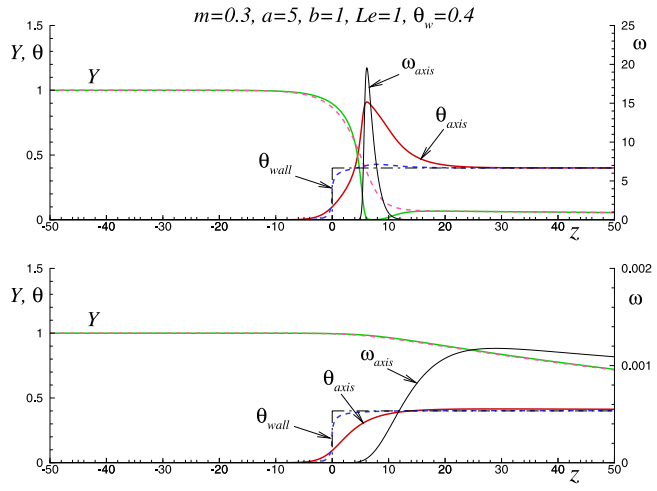

Fig. 9. Examples of the combustion mode (upper plot) and the slow reaction rate mode (lower plot) calculated for $m = 0.3$, $b = 1$ and $\theta_w = 0.4$. Solid and dashed lines correspond to distributions along the channel axis and near the wall, respectively.

as illustrated in Fig. 10. This also happens with the main eigenvalue corresponding to axisymmetric perturbations, $n = 0$. The dependencies of λ_R on m are shown for perturbations with azimuthal wave numbers $n = 0$ and $n = 1$, see Eq. (17), on Fig. 11. All curves were calculated for $Le = 1$, $b = 1$ and decreasing values of a. These curves are compared with that for the limiting case $a \to 0$. One can see that as a increases, the real part of the main eigenvalue, λ_R calculated for $n \geqslant 1$ becomes negative and the mode $n = 0$ determines the flame stability. Observe also that the narrow channel limit model (marked as $a \to 0$) approximates satisfactorily λ_R for the most unstable mode as $a \lesssim 1$ already. This allows to investigate effectively the stability properties within the one dimensional approximation. It should be remarked that this comparison is possible because Eq. (5) was used to define the heat transfer coefficient b.

The curves in Fig. 11 show that within a short segment of small values of m the values of λ remain real and negative. This segment is plotted in the inset of Fig. 11 with a dashed line for $a = 1$. As the flow rate increases, λ becomes complex (marked with an open circle in the inset), and, after this, λ_R becomes positive: the steady-state solution turns to be unstable. However with a further increase in the flow rate, the solution is re-stabilized. The re-stabilization points are marked in

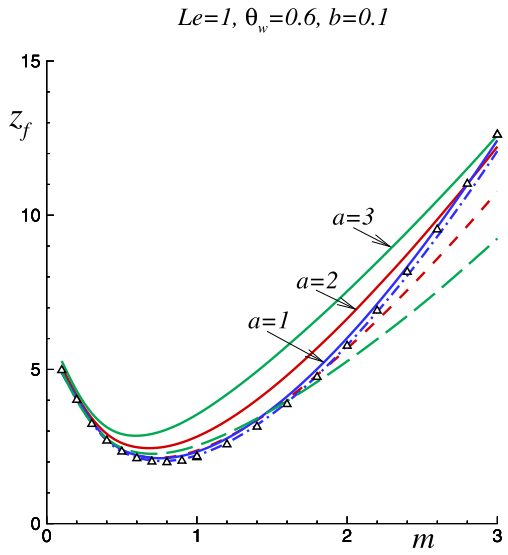

Fig. 10. The variation with m of the flame position on the axis z_f (solid lines for all a) and that at the channel wall z_f^w (long-dashed line for $a = 3$, dashed line for $a = 2$ and dash-dotted line for $a = 1$). The open triangles show the flame position in the limiting case of the narrow channel approximation based on Eqs. (12)–(13).

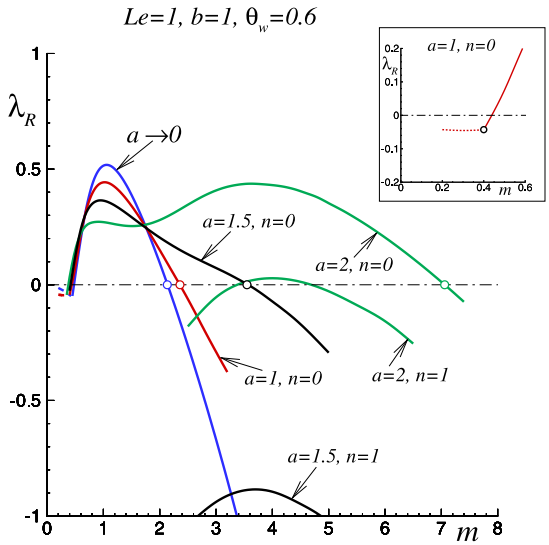

Fig. 11. Real parts of the main eigenvalues versus the flow rate calculated for channels with different cross-section radii and for the limiting case $a \to 0$; for $Le = 1$, $b = 1$ and $\theta_w = 0.6$. The inset shows the behavior of λ_R at small m for $a = 1$ and $n = 0$. For purely real values of λ, a dashed line is used, for λ_R with $\lambda_I > 0$, solid lines are used.

Fig. 11 with open circles. It should be noted that the re-stabilization flow rate increases rapidly with increasing channel radius and in order to get this effect at higher radii a significantly large value of m should be applied.

Numerical 3D simulations carried out using non-axisymmetric initial conditions revealed that for all cases with $Le = 1$ (at least for all the cases considered in this paper) the temperature and mass fraction distributions become axisymmetric after some time. This is explained by the fact that functions F_n defined by Eqs. (15)–(16) become about $\lesssim 10^{-12}$ for $n \geq 1$. Because of this, only the results of the axisymmetric simulations are presented below for $Le = 1$.

The time-dependent flame dynamics calculated for $m = 0.3$, 2 and 3 is presented in Fig. 12 for $a = 1$, $Le = 1$, $b = 1$ and $\theta_w = 0.6$ illustrating the re-stabilization effect. These calculations are in good agreement

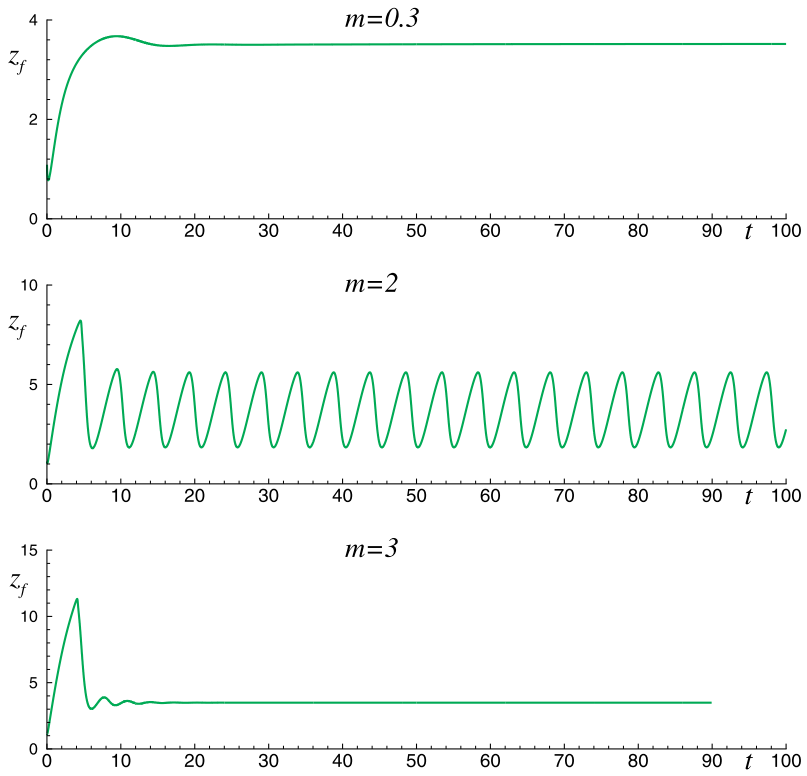

Fig. 12. Examples of time-dependent flame behavior illustrating the re-stabilization effect shown in Fig. 11, for $a = 1$, $Le = 1$, $b = 1$ and $\theta_w = 0.6$.

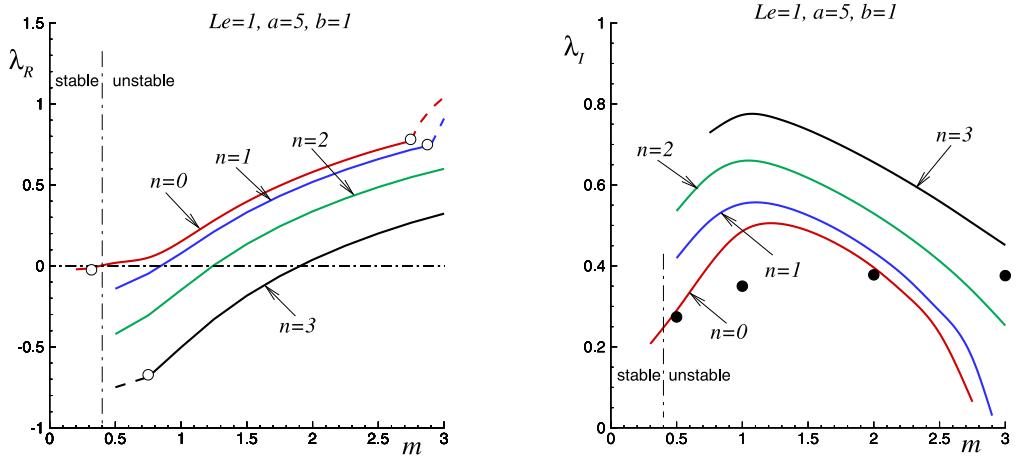

Fig. 13. Real (left plot) and imaginary (right plot) parts of the main eigenvalue calculated for the first four azimuthal wave numbers as a function of the flow rate m, for $a = 5$, $b = 1$, $\theta_w = 0.6$ and $Le = 1$. The segments on the left figure corresponding to $\lambda_I = 0$ are drawn with dashed lines and the transition points of the eigenvalue from an imaginary to a real number are marked with open circles. The black circles in the right plot show the oscillation frequencies obtained from time-dependent simulations based on Eqs. (1)–(2). The vertical dash-dotted line shows the stability boundary.

with the results of the linear stability analysis: the flame is stable at small m, then becomes oscillatory as m increases, and finally becomes stable again at sufficiently high flow rates.

Fig. 13 shows the real (left plot) and imaginary (right plot) parts of the main eigenvalue as functions of the flow rate m for different modes with $n = 0$, 1, 2 and 3. All curves are calculated for larger channel radii, $a = 5$, $b = 1$ and $\theta_w = 0.6$. The segments shown with dashed and solid lines in the left plot correspond to the eigenvalues with $\lambda_I = 0$ and $\lambda_I > 0$, respectively. Open circles indicate the transition points.

This figure shows that, as for small a, the steady-state axisymmetric solution is stable at low flow rates. With a gradual increase in m, the eigenvalue for $n = 0$ first becomes imaginary and then its real part passes to the right half-plane of the complex λ plane, that is, Hopf's bifurcation occurs. This critical flow rate value is marked by vertical dash-dotted lines on both figures. One can see that λ_R for eigenvalues with $n > 0$ becomes also positive with increasing values of m, but its magnitude remains always less than that for $n = 0$. It means that the modes with $n > 0$ are less unstable than the axisymmetric mode $n = 0$. Another distinctive feature that appears at large radii is that the principal eigenvalues become purely real for sufficiently high m, as shown by the dashed lines in Fig. 13.

The real part of the main eigenvalue of the axisymmetric mode is given also in Fig. 14 for $a = 3$ and $a = 8$ showing that λ_R calculated for $n = 0$ exceeds that for $n > 0$. These results indicate that for $Le = 1$, the flame oscillations are determined by the axisymmetric mode $n = 0$, at least for the considered range of parameters.

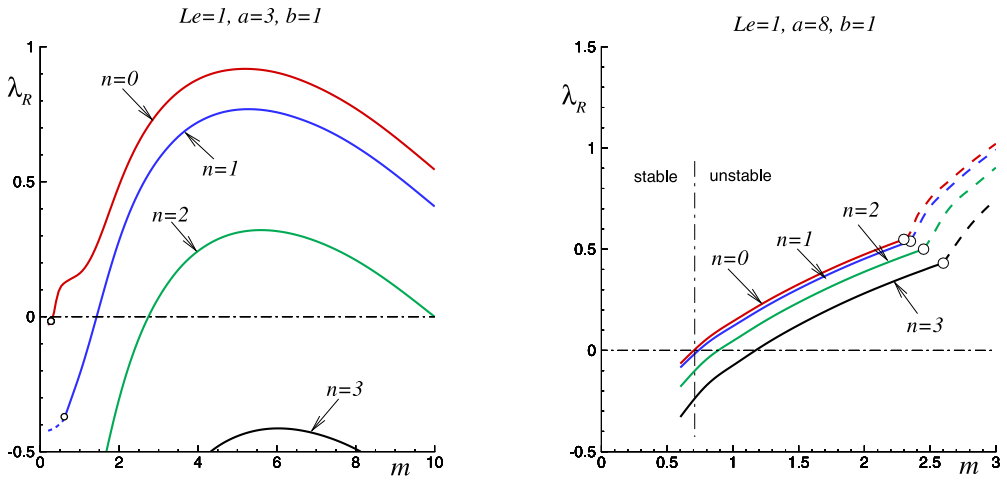

Fig. 14. The main eigenvalues real parts for different modes as a function of flow rate calculated for $Le = 1$, $b = 1$, $a = 3$ (left panel) and $a = 8$ (right panel). Dashed lines correspond to purely real eigenvalues, for solid lines $\lambda_I \neq 0$.

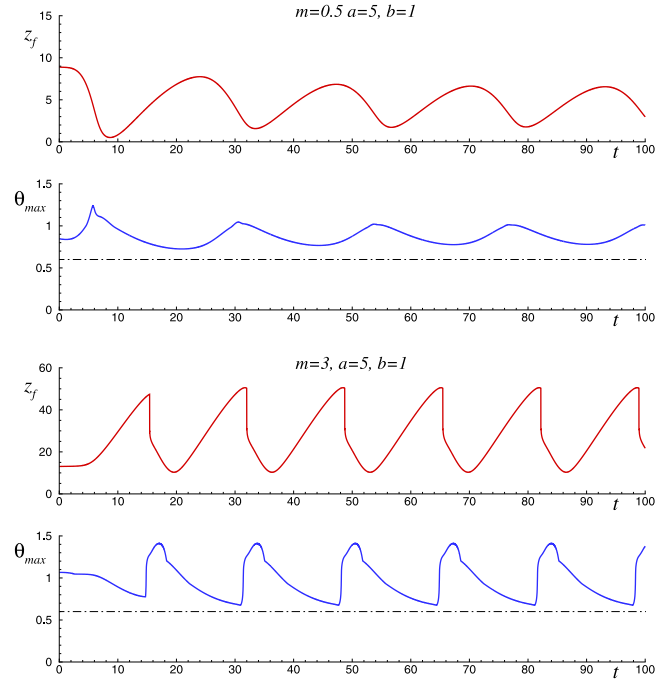

Fig. 15. Time histories of the flame position on the channel axis and the maximum temperature in the domain for the case with $Le = 1$, $a = 5$ and $b = 1$. The curves in the top two plots are calculated for $m = 0.5$ (close to the lower limit of instability) and in the bottom two plots for $m = 3$ (in the zone with a purely real eigenvalue).

The results obtained for circular channels differ from those for planar channels (slots) reported in [25]. In that paper, it was found that in the planar channel when the flow rate exceeds a certain critical value, the non-symmetric perturbations of flames with $Le = 1$ become more unstable than the symmetric ones. This led to the emergence of non-symmetric flame dynamics in a slot. If we draw an analogy associating the modes with $n \geq 1$ (in a circular channel) with the non-symmetric modes in a slot, then one can see a clear difference between these two cases.

The time histories of the flame position and the maximum temperature reached in the domain are shown in Fig. 15 for $m = 0.5$ and $m = 3$ calculated with $a = 5$, $b = 1$, $Le = 1$ and $\theta_w = 0.6$. The oscillation frequencies calculated numerically for these and other flow rates are shown in Fig. 13 (right plot) with dark circles. For the first case, $m = 0.5$, the flow rate exceeds slightly the critical value above which the flame becomes unstable. Although the amplitude of the oscillations is noticeable, the frequency evaluated using the time-dependent simulations is close to λ_I obtained from the linear stability analysis. However, as the flow rate increases, an appreciable difference appears between the frequencies of time dependent simulations and λ_I. This is especially evident for the case with $m = 3$ for which $\lambda_I = 0$ for the $n = 0$ mode, and, in contradiction, the flame shows oscillations in the simulations. This can be attributed to a repetitive extinction and ignition regime (FREI) when the flame is first carried away downstream from the beginning of the heating zone, almost blows away, but then a process of re-ignition occurs followed by a flame motion upstream. Figs. 13 and 15 clearly indicate that the flame instability obtained from the linear analysis, namely when we have $\lambda_R > 0$, only indicates that the steady-state solution is unstable. The specific implementation of unstable dynamics cannot be predicted.

5.2. Flames with $Le < 1$

The instabilities for flames with $Le = 1$ described above arise solely due to the channel heating. Indeed, the Darrieus–Landau instability does not take place within the constant density model and the differential diffusion effect is also excluded for $Le = 1$. However this is not the case for flames with the Lewis number not equal to one. It is well known that thermo-diffusive instabilities of a planar flame front lead to a cellular structure for $Le < 1$ with no oscillations: the imaginary part of the eigenvalue remains always equal to zero, $\lambda_I = 0$, see, for example, [35,36]. The results presented below show that in the case of flames in channels with heating, a combination of the cellular instability and the heating-induced instability occurs.

Fig. 16 shows λ_R calculated for various modes with different n plotted versus the flow rate for $a = 5$, $Le = 0.7$ and two values of the heat exchange coefficient, $b = 0.3$ (left plot) and $b = 1$ (right plot). As in previous figures, solid lines indicate the eigenvalues with $\lambda_I \neq 0$ while dashed lines correspond to a purely real eigenvalue. It can be seen that with an increase in the flow rate the axisymmetrical mode, $n = 0$, becomes unstable first and that this mode has an oscillatory nature ($\lambda_I \neq 0$). However, with an increase in the flow rate, cellular instability modes ($\lambda_I = 0$) with $n > 0$ begin to prevail and the wave number of the most unstable mode increases with m. It is interesting that for $b = 0.3$ (left plot) the mode with $n = 4$ becomes the most unstable one, whereas for $b = 1$ the most unstable mode has $n = 3$. As various calculations showed, this trend (an increase of the wave number of the most unstable mode with m) has a universal character for flames with $Le < 1$.

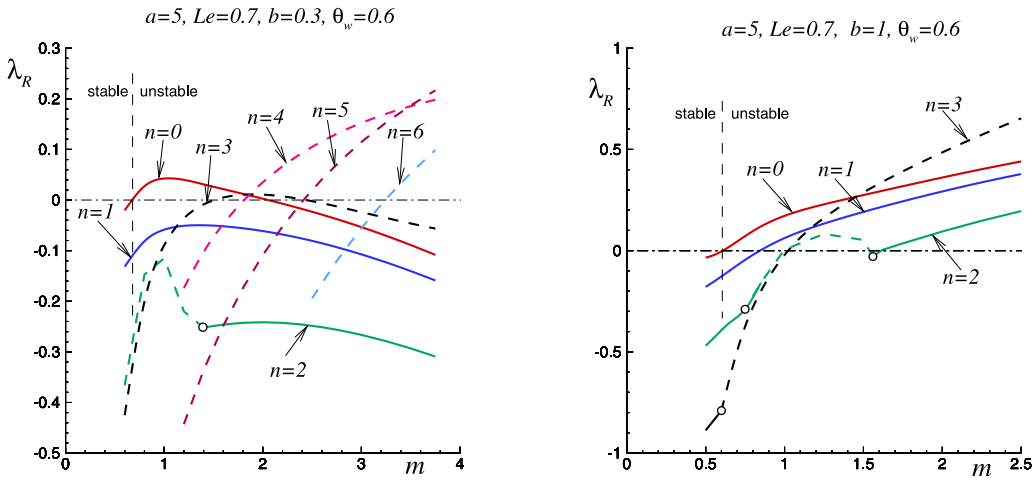

Fig. 16. Real parts of the main eigenvalue for different modes as a function of flow rate calculated for $Le = 0.7$, $a = 5$, $b = 0.3$ (left panel) and $b = 1$ (right panel). Dashed lines correspond to purely real eigenvalues, for solid lines $\lambda_I \neq 0$.

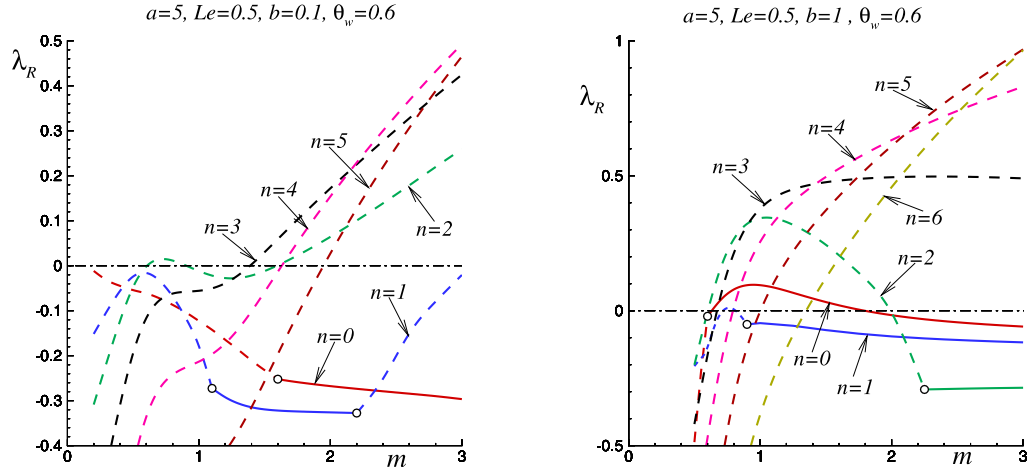

Fig. 17. Real parts of the main eigenvalue for different modes as a function of flow rate calculated for $Le = 0.5$, $a = 5$, $b = 0.1$ (left panel) and $b = 1$ (right panel). Dashed lines correspond to purely real eigenvalues, for solid lines $\lambda_I \neq 0$.

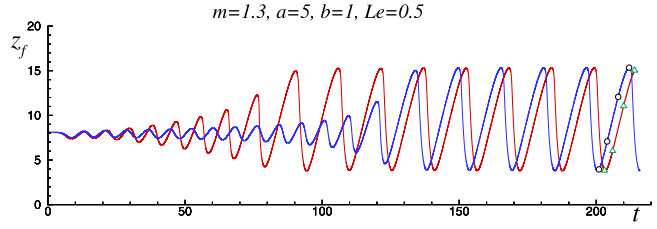

Fig. 18. Time history of the flame position in the center of the channel, z_f, for $m = 1.3$, $a = 5$, $b = 1$, $Le = 0.5$. Calculations were initiated from the axisymmetric steady-state subjected to two different small non-axisymmetric perturbations imposed on the temperature field. Open circles and triangles correspond to the distributions shown in Figs. 19 and 20.

It can be expected that at even lower Lewis numbers, cellular instability becomes dominant. This is illustrated in Fig. 17 for $Le = 0.5$ where the real parts of principal eigenvalues are shown for different modes calculated for $a = 5$. The left plot corresponds to a low value of the heat transfer coefficient, $b = 0.1$, and the right one to $b = 1$. One can see in the left figure that almost all curves (those shown with dashed lines) correspond to purely real eigenvalues, $\lambda_I = 0$. The only exceptions are the modes $n = 0$ and $n = 1$ for which there are segments with $\lambda_I \neq 0$ (solid lines), but these modes do not affect the linear stability since $\lambda_R < 0$.

The curves shown in the right plot of Fig. 17 were calculated for a larger value of the heat transfer coefficient, $b = 1$. It can be seen that the loss of flame stability occurs for increasing m due to the cellular modes ($\lambda_I = 0$). Nevertheless, the figure shows also that the axisymmetric ($n = 0$) perturbation mode still has also $\lambda_R > 0$ and $\lambda_I \neq 1$ for the corresponding segment is drawn with a solid line. This means that the cellular instability and the axisymmetric oscillatory instability occur simultaneously.

The numerical results based on three-dimensional simulations presented below showed that for $Le < 1$ a multiplicity of time-dependent solutions can take place. When this multiplicity happens, the flame dynamics depends on the initial conditions. Obviously, it is impossible to enumerate all possible situations. For this reason, the results presented below perhaps cover only a subset of possible flame dynamics.

Fig. 18 presents two cases of the flame position history (the position of the point with maximum ω at the channel axis) for $m = 1.3$, $a = 5$, $b = 1$ and $Le = 0.5$. As initial condition for the calculations, an axisymmetric steady-state distribution for the mass fraction and temperature was chosen to which two different small temperature perturbations were superimposed. The smallness of the perturbation amplitude ensures that during a certain period of time the deviation of the flame position from its steady state value remains small, as can

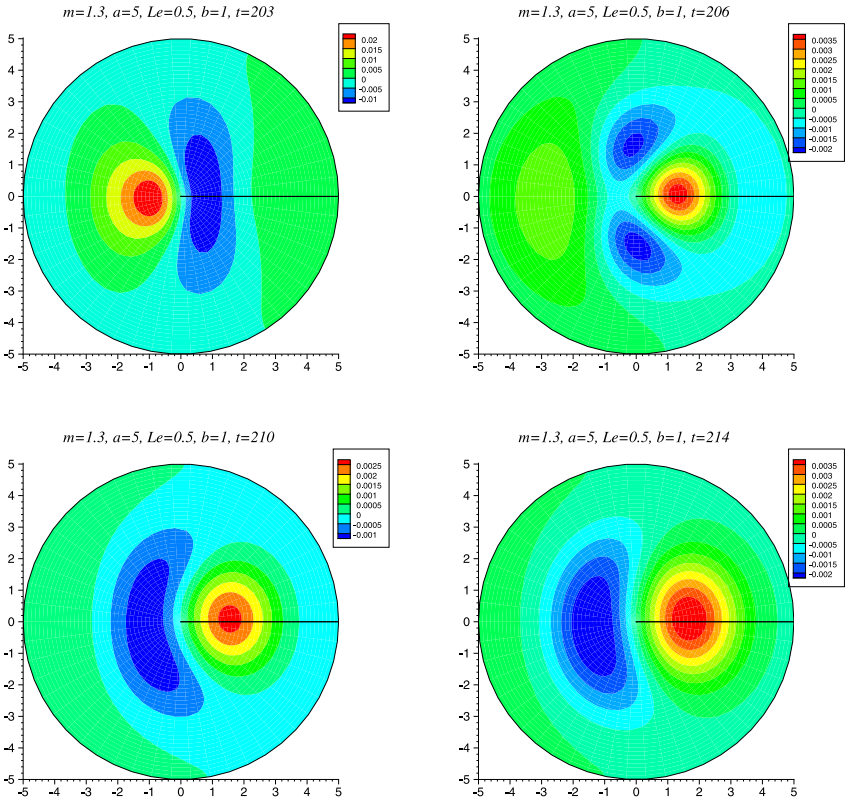

Fig. 19. An illustration of the cellular structure of the flame shown for $\theta - \overline{\theta}$ appearing during the flame oscillation process; distributions corresponding to the points indicated by the open circles in Fig. 18.

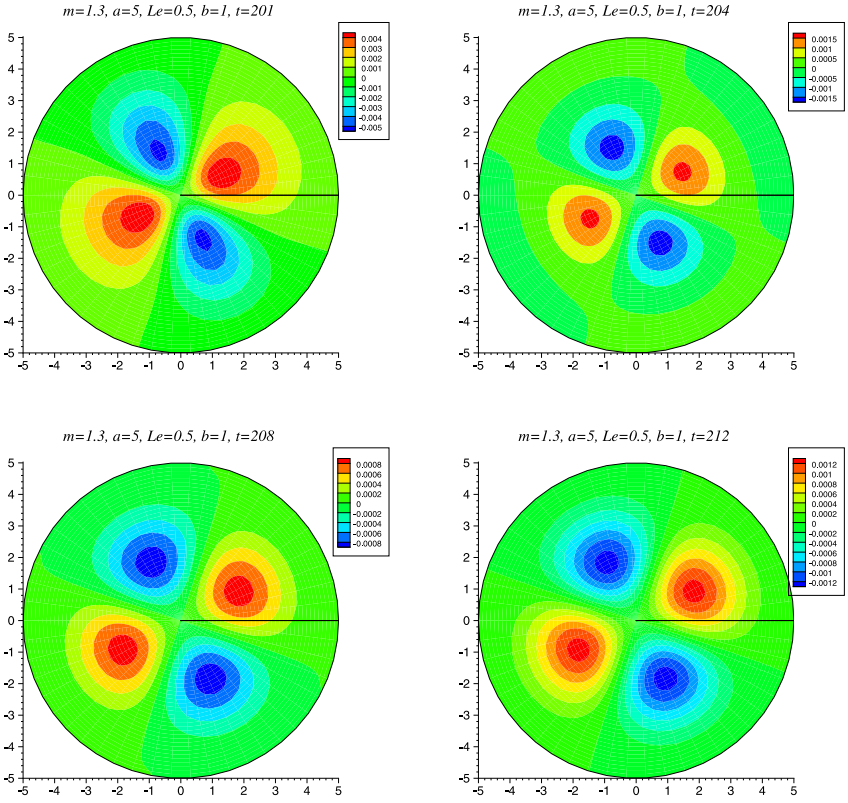

Fig. 20. An illustration of the cellular structure of the flame shown for $\theta - \overline{\theta}$ appearing during the flame oscillation process; distributions corresponding to the points indicated by the open triangles in Fig. 18.

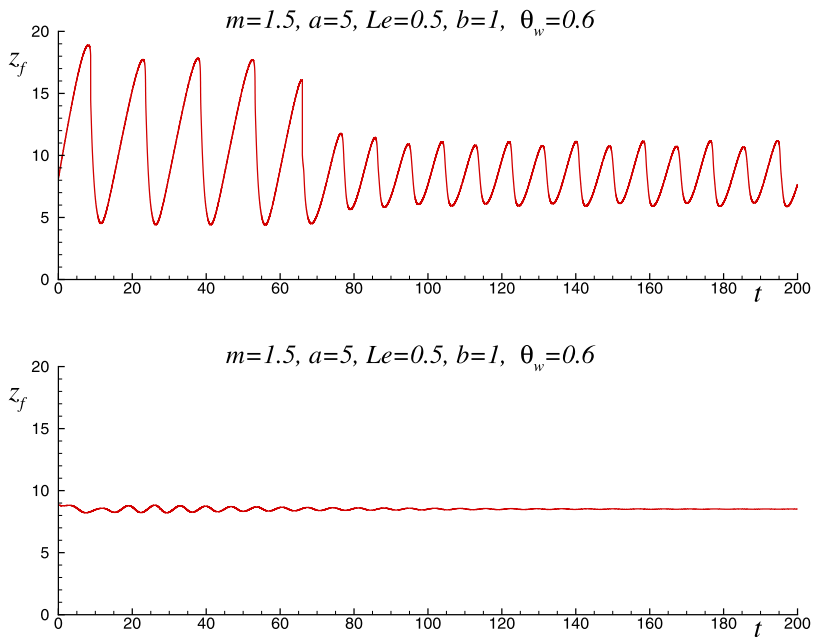

Fig. 21. An example of two different flame dynamics identified for the same set of parameters. The top plot shows the oscillatory dynamics, in the bottom plot the flame ceases to oscillate and the cellular structure becomes dominant.

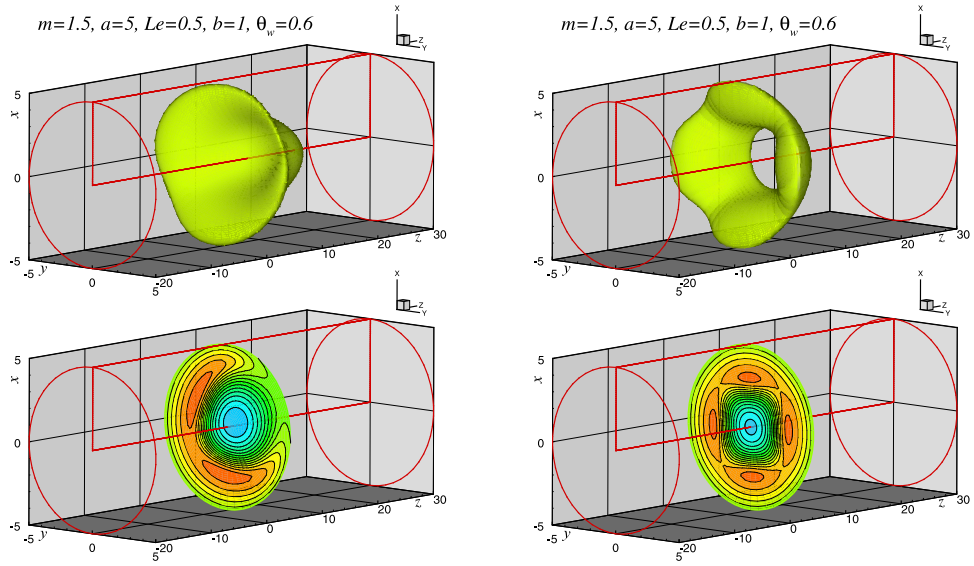

Fig. 22. Example of temperature iso-surface and temperature distribution in section $z = z_f$; left plots illustrate the oscillatory dynamics, right plots show the time independent cellular structure.

be seen from the figure at $t \lesssim 10$. It is also seen that the further dynamics of the flame becomes different (for $10 \lesssim t \lesssim 150$) for these two cases. At large times, the oscillations of z_f become similar in amplitude. However, a more detailed analysis showed that the flame structures are different for these two cases.

In order to highlight the differences in the structure of the flames more clearly, Figs. 19 and 20 show the distributions of $\theta - \overline{\theta}$, where $\overline{\theta}$ is the φ-averaged temperature defined in Eq. (15). All plots are drawn for sections $z = z_f(t)$ and correspond to open circles and open triangles indicated in Fig. 18. It is clearly seen that the flame structures reveal two different types of cells for these two cases. Indeed, Fig. 19 shows the structure corresponding to the $n = 1$ mode, while in Fig. 20 the cellular structure corresponds to $n = 2$.

Although the structures of the flames obtained for $m = 1.3$ are clearly different, the values of $\theta - \bar{\theta}$ shown in Figs. 19 and 20 are quite small. However, it turns out that for larger values of m, the differences in structure and dynamics can be more significant. Fig. 21 shows two cases obtained for $m = 1.5$. The upper plot demonstrates the oscillatory flame dynamics while the lower case shows the dynamics leading to a time-independent cell structure after a transitional period of time. The corresponding temperature distribution snapshots for these two cases are shown in Fig. 22, where the temperature iso-surfaces and temperature distributions are shown. The left drawings illustrate the oscillatory mode in which the cellular structure of the flame is also clearly visible while the right plots show the final four-cell steady-state time-independent structure.

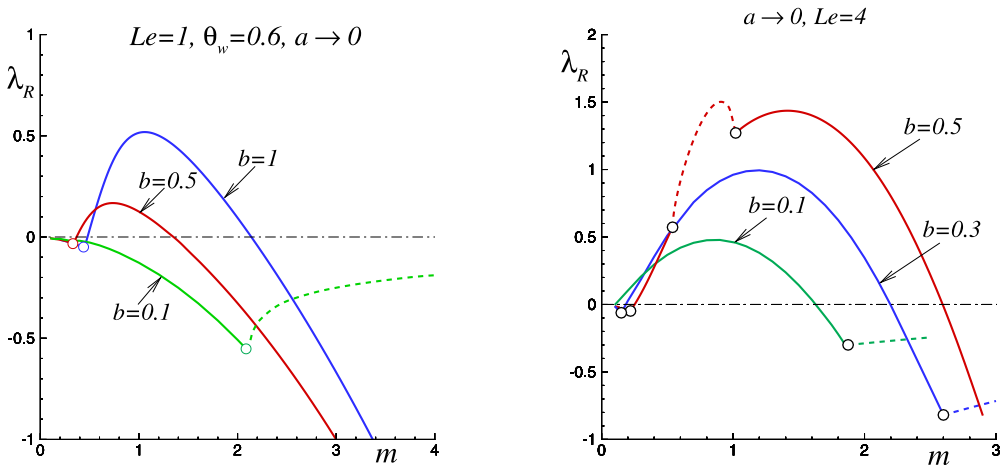

Fig. 23. Real parts of the principal eigenvalue plotted versus m for various b calculated in the limit $a \to 0$, for $Le = 1$ (left plot) and $Le = 4$ (right plot). Dashed lines correspond to purely real eigenvalues, for solid lines $\lambda_I \neq 0$.

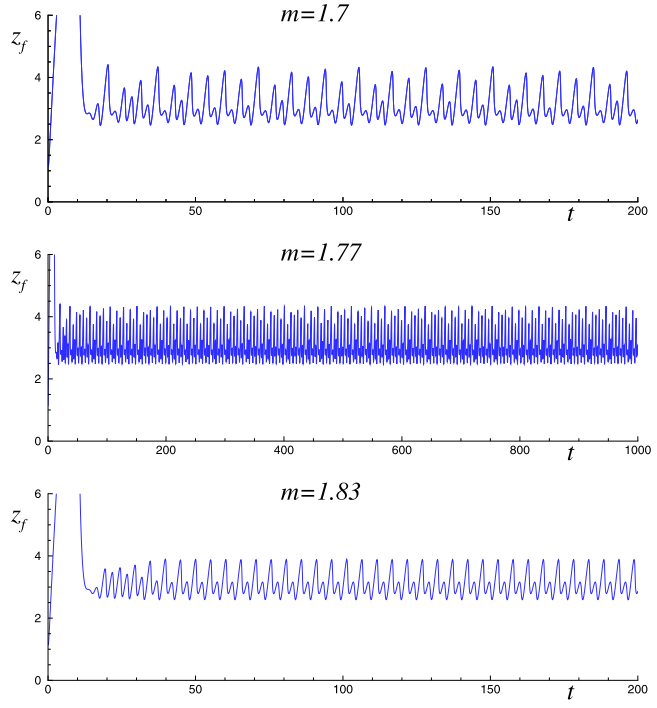

Fig. 24. Time histories of the flame position for the case of $Le = 4$, $b = 0.3$ and $a \to 0$ at different values of the flow rate m.

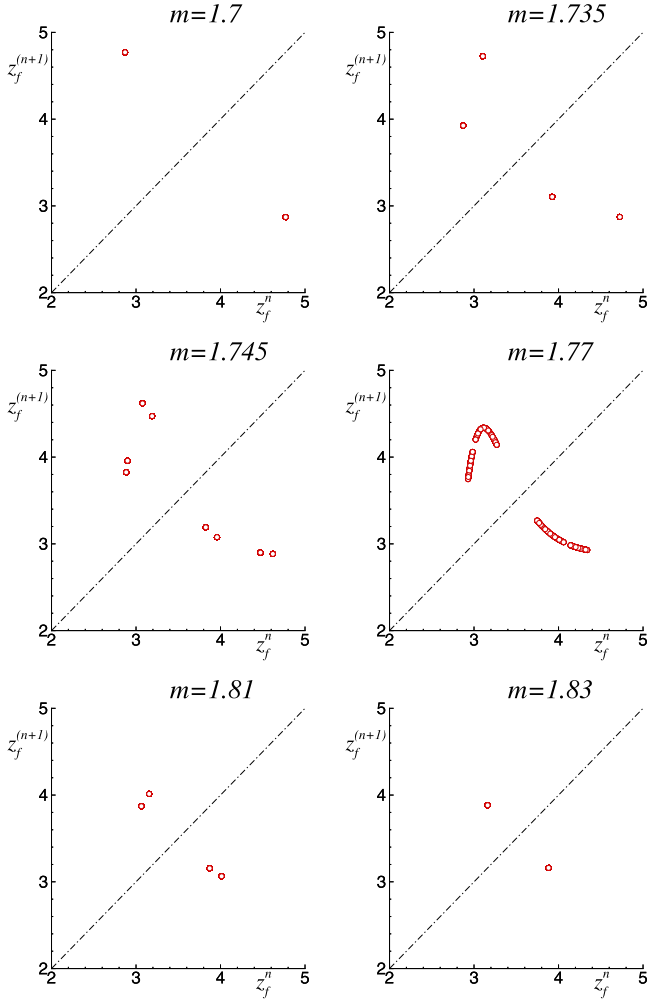

Fig. 25. The first return map of the relative maximum z_f plotted for $Le = 4$, $b = 0.3$ and various m. The figure illustrates the appearance of the forward and reverse Feigenbaum cascades with a gradual increase in the flow rate.

5.3. Flames with $Le > 1$

Just as for flames with $Le < 1$, when the oscillatory instability caused by the heating of the channel walls is mixed with the intrinsic cellular thermal-diffusion instability that occurs at low Lewis numbers, for flames with $Le > 1$ the flame instability caused by heating is combined with the intrinsic oscillatory thermo-diffusive instability. As shown below, this effect can cause chaotic flame behavior.

Numerical three-dimensional simulations carried out for $Le > 1$ showed that, as for cases with $Le = 1$, the resulting flames turn out to be axisymmetric, at least in the considered range of parameters. For this reason, the results obtained for Lewis number greater than one are focused below on axisymmetric flames.

Fig. 23 compares the stability curves obtained in the limit $a \to 0$ for $Le = 1$ (left plot) and $Le = 4$ (right plot) and various b. Solid curves correspond to eigenvalues with nonzero imaginary part, while for dashed curves $\lambda_I = 0$. The transition points are indicated by open circles. It can be seen that the stability curves look similar, although

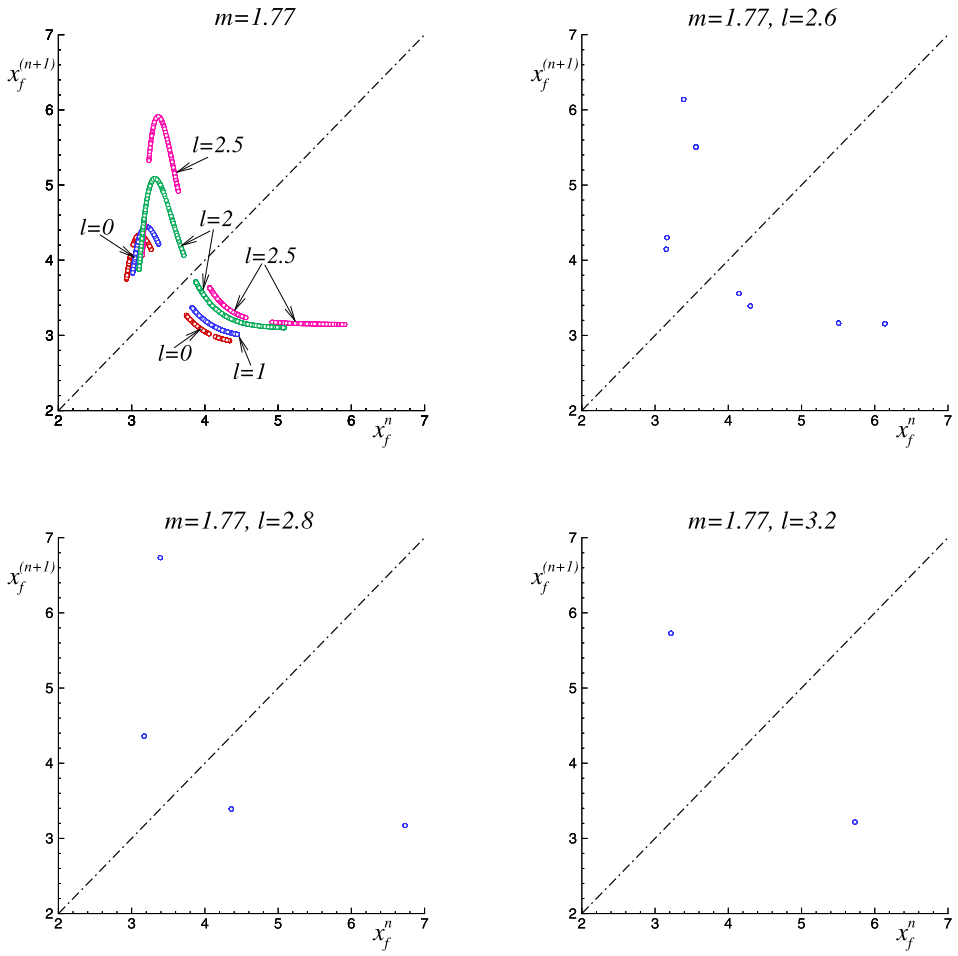

Fig. 26. The first return map of the relative maximum z_f plotted for $Le = 4$, $b = 0.3$, $m = 1.77$ and different values of the parameter ℓ appearing in Eq. (10) which determines the outer wall temperature profile $\theta_W(z)$.

one should note the appearance of an interval of real eigenvalues for $b = 0.5$ and $Le = 4$.

Fig. 24 shows examples of the time histories of the flame position calculated for $Le = 4$, $b = 0.3$ and three values of the flow rate. It can be seen that at $m = 1.7$ and $m = 1.83$ an oscillatory dynamics of the flame is observed, while for an intermediate value $m = 1.77$ the behavior of the flame is disordered.

Variations of the flame dynamics are investigated with the first return map technique. Using the dependence of the flame position versus time the series of the local maxima of z_f are identified, $\{z_{fn}, n = 1, 2, \dots\}$, where n is the maximum number. The dependence $z_{f(n+1)}$ versus z_{fn} is plotted in Fig. 25 for $b = 0.3$ and various m. These plots were created using $n > 100$ after the starting of simulations, in order to allow the flame dynamics to approach the corresponding attractor.

Fig. 25 shows only the selected first return cards. However, it can be seen that the simple periodic dynamics observed for $m = 1.7$ experiences successive bifurcations of the Feigenbaum cycle doubling with a gradual increase in the flow rate. At $m = 1.77$, the first return map becomes continuous (four continuous parts), indicating chaotic behavior. However, with a further increase in the flow rate, the reverse Feigenbaum cascade occurs and the flame dynamics returns to simple oscillatory behavior. It is interesting to note that the stability curve shown in Fig. 23 for $b = 0.3$ does not have any features in the vicinity of the value $m = 1.77$.

In order to be sure that the emergence of a chaotic flame behavior is a stable trend, and is not caused, for example, by a specific profile of the outer wall temperature, numerical simulations were carried out imposing the outer wall temperature according to Eq. (10). In this case, the temperature profile is continuous and the width of the temperature change interval is determined by the parameter ℓ. Fig. 26 compares the first return maps for various ℓ calculated for $Le = 4$ and $m = 1.77$. It is clearly seen that the chaotic behavior of the flame is enhanced in a certain sense, namely, for $\ell = 2$, the first return map consists of two continuous parts (the upper left plot), and not four, as for the case with $\ell = 0$. However, for larger values of ℓ, the reverse cascade of cycle doubling occurs, as can be seen from the other figures in Fig. 26.

6. Conclusions

Combustion problems are typically non-linear, a characteristic linked to the non-linear chemical reaction rate dependence on temperature, or the non-linearity of the flame–wall interactions, among other effects. As a consequence of non-linearity, several steady and dynamic modes may appear as solutions of the problem for a single set of parameters, and several of them may be simultaneously stable. The actual realization of one or another of the stable modes depends on the initial conditions. For this reason, the experimental verification of the existence of multiple modes might be difficult, given that initial conditions (for example, ignition) are not always easy to control. This is why the role of mathematical modeling becomes important in the study of the multiplicity phenomenon.

In this work, we showed that multiple modes can occur even in the fairly simple configuration of a flame in a channel with a partially heated wall. For flames with fuel Lewis number smaller than one, the combination of cellular instabilities with the instability caused by the heating of the channel walls can lead to several different simultaneous

dynamic regimes. For Lewis number greater than one, oscillations induced by thermo-diffusive instabilities and from the heating of the wall result in complex oscillatory dynamics. In this last case, we showed that the oscillatory dynamics can even become chaotic, at least for a narrow parametric region.

We should mention that a number of simplifications were made in the study, in order to obtain a relatively simple model for which a parametric study together with a stability analysis were feasible. The authors believe that if some phenomena are observed in simplified models, then they are likely to occur within more complete models. A recent example of this is our study of flame symmetry breaking in circular channels in [28,32]. This phenomenon was first studied within the framework of a constant density model in [28], and then it was shown that for a variable density model based on the full Navier–Stokes equations qualitatively similar results were obtained [32]. The present study demonstrates clearly that when the channel is partially heated, the multiple combustion modes can appear. It can be expected that, when the simplifying assumptions are relaxed, at least some of these effects will be preserved. This will be the object of further studies.

CRediT authorship contribution statement

Vadim N. Kurdyumov: Investigation, Writing – original draft, Writing – review & editing. **Daniel Fernández-Galisteo:** Investigation, Writing – original draft, Writing – review & editing. **Carmen Jiménez:** Investigation, Writing – original draft, Writing – review & editing.

Declaration of competing interest

The authors declare that they have no known competing financial interests or personal relationships that could have appeared to influence the work reported in this paper.

Acknowledgments

This study was supported by MCIN with funding from European Union NextGenerationEU (PRTR-C17.I1) as well by grants #TED2021-129446-C42/MCIN/AEI/10.13039/501100011033/NextGenerationEU/PRTR and #PID2022-139082NB-C52 MCIN/ AEI /10.13039/501100011033/ and FEDER.

References

[1] A.C. Fernández-Pello, Micropower generation using combustion: issues and approaches, Proc. Combust. Inst. 29 (2002) 883–899.
[2] Y. Ju, K. Maruta, Microscale combustion: technology development and fundamental research, Prog. Energy Combust. Sci. 37 (2011) 669–715.
[3] J.L. Ellzey, E.L. Belmont, C.H. Smith, Heat recirculating reactors: Fundamental research and applications, Prog. Energy Combust. Sci. 72 (2019) 32–58.
[4] N.S. Kaisare, D.G. Vlachos, A review on microcombustion: fundamentals, devices and applications, Prog. Energy Combust. Sci. 38 (2012) 321–359.
[5] Y. Ju, C.W. Choi, An analysis of sub-limit flame dynamics using opposite propagating flames in mesoscale channels, Combust. Flame 133 (2003) 483–493.
[6] R.V. Fursenko, S.S. Minaev, Flame stability in a system with counterflow heat exchange, Combust. Explos. Shock Waves 41 (2) (2005) 133–139.
[7] I. Schoegl, J.L. Ellzey, Superadiabatic combustion in conducting tubes and heat exchangers of finite length, Combust. Flame 151 (2007) 142–159.
[8] V.N. Kurdyumov, M. Matalon, Analysis of an idealized heat-recirculating microcombustor, Proc. Combust. Inst. 33 (2) (2011) 3275–3284.
[9] V.N. Kurdyumov, D. Fernández-Galisteo, C. Jiménez, Superadiabatic small-scale combustor with counter-flow heat exchange: Flame structure and limits to narrow-channel approximation, Combust. Flame 222 (2020) 233–241.
[10] J. Bosch, D. Fernández-Galisteo, C. Jiménez, V.N. Kurdyumov, Analytical study of superadiabatic small-scale combustors with a two-step chain-branching chemistry model: lean burning below the flammability limit, Combust. Flame 235 (2022) 11173.
[11] J. Bosch, D. Fernández-Galisteo, C. Jiménez, V.N. Kurdyumov, Superadiabatic small-scale combustors: Asymptotic analysis of a two-step chain-branching combustion model, Proc. Combust. Inst. 39 (2023) 1927–1935.
[12] J. Bosch, D. Fernández-Galisteo, C. Jiménez, V.N. Kurdyumov, Small-scale superadiabatic combustors with a two-step chain-branching chemistry model: Asymptotic models and the effect of two-dimensionality on lean mixtures burning, Combust. Flame 259 (2024) 113127.
[13] D. Fernández-Galisteo, E. Fernández-Tarrazo, C. Jiménez, V.N. Kurdyumov, Analysis of an idealized counter-current microchannel-based reactor to produce hydrogen-rich syngas from methanol, Int. J. Hydr. Eng. 44 (2019) 23807–23820.
[14] K. Maruta, T. Kataoka, N.I. Kim, S. Minaev, R. Fursenko, Characteristics of combustion in a narrow channel with a temperature gradient, Proc. Combust. Int. 30 (2005) 2429–2436.
[15] M. Hori, H. Nakamura, T. Tezuka, S. Hasegawa, K. Maruta, Characteristics of n-heptane and toluene weak flames in a micro flow reactor with a controlled temperature profile, Proc. Combust. Int. 34 (2013) 3419–3426.
[16] T. Kamada, H. Nakamura, T. Tezuka, S. Hasegawa, K. Maruta, Study on combustion and ignition characteristics of natural gas components in a micro flow reactor with a controlled temperature profile, Combust. Flame 161 (2014) 37–48.
[17] H. Nakamura, S. Suzuki, T. Tezuka, S. Hasegawa, K. Maruta, Sooting limits and PAH formation of n-hexadecane and 2 2, 4 4, 6 8, 8-heptamethylnonane in a micro flow reactor with a controlled temperature profile, Proc. Combust. Int. 35 (2015) 3397–3404.
[18] S. Takahashi, H. Nakamura, T. Tezuka, S. Hasegawaa, K. Maruta, Multi-stage oxidation of a CH2F2/air mixture examined by weak flames in a micro flow reactor with a controlled temperature profile, Combust. Flame 201 (2019) 140–147.
[19] A.K. Dubeya, T. Tezukaa, S. Hasegawaa, H. Nakamuraa, K. Maruta, Analysis of kinetic models for rich to ultra-rich premixed CH4/air weak flames using a micro flow reactor with a controlled temperature profile, Combust. Flame 206 (2019) 68–82.
[20] M.H.B. Hanafia, H. Nakamura, S. Hasegawa, T. Tezuka, K. Maruta, Effects of n-butanol blends on the formation of hydrocarbons and PAHs from fuel-rich heptane mombustion in a micro flow reactor with a controlled temperature profile, Combust. Sci. Tech. 193 (2021) 2085–2110.
[21] K. Akita, Y. Morii, Y. Murakami, H. Nakamura, T. Tezuka, K. Maruta, Dynamics of FREI with/without cool flame interaction, Proc. Combust. Int. 39 (2023) 1957–1965.
[22] G. Pizza, C.E. Frouzakis, J. Mantzaras, A.G. Tomboulides, K. Boulouchos, Dynamics of premixed hydrogen/air flames in microchannels, Combust. Flame 152 (2008) 433–450.
[23] G. Pizza, C.E. Frouzakis, J. Mantzaras, A.G. Tomboulides, K. Boulouchos, Three-dimensional simulations of premixed hydrogen/air flames in microtubes, J. Fluid Mech. 658 (2010) 463–491.
[24] V.N. Kurdyumov, G. Pizza, C.E. Frouzakis, J. Mantzaras, Dynamics of premixed flames in a narrow channel with a step-wise wall temperature, Combust. Flame 156 (2009) 2190–2200.
[25] V.N. Kurdyumov, D. Fernández-Galisteo, C. Jiménez, Premixed flames in a narrow slot with a step-wise wall temperature: linear stability analysis and dynamics, Combust. Theor. Model. 25 (2021) 1132–1157.
[26] V.N. Kurdyumov, C. Jiménez, Flame stabilization in narrow channels by a highly conductive wall segment: Application to small-scale combustion devices, Combust. Flame 245 (2022) 112348.
[27] V.N. Kurdyumov, C. Jiménez, V.V. Gubernov, A.V. Kolobov, Global stability analysis of gasless flames propagating in a cylindrical sample of energetic material: Influence of radiative heat losses, Combust. Flame 162 (2015) 1996–2005.
[28] V.N. Kurdyumov, C. Jiménez, Structure and stability of premixed flames propagating in narrow channels of circular cross-section: Non-axisymmetric, pulsating and rotating flames, Combust. Flame 167 (2016) 149–163.
[29] V.N. Kurdyumov, C. Jiménez, Propagation of symmetric and non-symmetric premixed flames in narrow channels: Influence of conductive heat-losses, Combust. Flame 161 (2014) 927–936.
[30] W.B. Bush, F.E. Fendell, Asymptotic analysis of laminar flame propagation for general lewis number, Combust. Sci. Tech. 1 (1970) 421–428.
[31] V.N. Kurdyumov, Lewis number effect on the propagation of premixed flames in narrow adiabatic channels: Symmetric and non-symmetric flames and their linear stability analysis, Combust. Flame 158 (2011) 1307–1317.
[32] A. Dejoan, V.N. Kurdyumov, Thermal expansion effect on the propagation of premixed flames in narrow channels of circular cross-section: Multiplicity of solutions, axisymmetry and non-axisymmetry, Proc. Combust. Int. 37 (2019) 1827–1935.
[33] V.N. Kurdyumov, M. Matalon, The porous-plug burner: Flame stabilization, onset of oscillation, and restabilization, Combust. Flame 153 (2008) 105–118.
[34] V.N. Kurdyumov, M. Sánchez-Sanz, Influence of radiation losses on the stability of premixed flames on a porous-plug burner, Proc. Combust. Int. 34 (2013) 989–996.
[35] Ya.B. Zel'dovich, G.I. Barenblatt, V.B. Librovich, G.M. Mahkviladze, The Mathematical Theory of Combustion and Explosions, Consultants Bureau, New York, 1985.
[36] G. Sivashinsky, Diffusional-thermal theory of cellular flames, Combust. Sci. Tech. 15 (1977) 137–146.